Astronomy & Astrophysics manuscript no. GRB090205˙AA˙accepted
June 7, 2010

The afterglow and host galaxy of GRB 090205: evidence for a Ly–α emitter at $z = 4.65^{\star}$

P. D'Avanzo[1], M. Perri[2], D. Fugazza[1], R. Salvaterra[3], G. Chincarini[1,4], R. Margutti[1,4], X. F. Wu[5,6,7], C. C. Thöne[1], A. Fernández-Soto[8], T. N. Ukwatta[9,10], D. N. Burrows[5], N. Gehrels[10], P. Meszaros[5,6,11], K. Toma[5,6], B. Zhang[12], S. Covino[1], S. Campana[1], V. D'Elia[2,13], M. Della Valle[14,15], and S. Piranomonte[13]

[1] INAF-Osservatorio Astronomico di Brera, via Bianchi 46, I-23807, Merate, Italy.
[2] ASI Science Data Center, via Galileo Galilei, I-00044, Frascati, Italy.
[3] Università degli Studi dell'Insubria, Dipartimento di Fisica e Matematica, via Valleggio 11, I-22100, Como, Italy.
[4] Università degli Studi di Milano-Bicocca, Dipartimento di Fisica, piazza delle Scienze 3, I-20126, Milano, Italy.
[5] Department of Astronomy and Astrophysics, Pensylvania State University, 525 Davey Lab, University Park, PA 16802, USA.
[6] Center for Particle Astrophysics, Pensylvania State University.
[7] Purple Mountain Observatory, Chinese Academy of Sciences, Nanjing 210008, China.
[8] Instituto de Física de Cantabria (CSIC-UC), 39005, Santander, Spain.
[9] The George Washington University, Washington, D.C., 20052, USA.
[10] NASA/Goddard Space Flight Center, Greenbelt, MD 20771, USA.
[11] Department of Physics, Pensylvania State University.
[12] Department of Physics and Astronomy, University of Nevada, Las Vegas, NV 89154, USA.
[13] INAF-Osservatorio Astronomico di Roma, via di Frascati 33, I-00040, Monteporzio Catone (Roma), Italy.
[14] INAF-Osservatorio Astronomico di Capodimonte, salita Moiariello 16, I-80131 Napoli, Italy.
[15] International Center for Relativistic Astrophysics, piazza della Repubblica 10, I-65122, Pescara, Italy.

Received; accepted

ABSTRACT

Aims. Gamma-ray bursts have been proved to be detectable up to distances much larger than any other astrophysical object, providing the most effective way, complementary to ordinary surveys, to study the high redshift universe. To this end, we present here the results of an observational campaign devoted to the study of the high–z GRB 090205.
Methods. We carried out optical/NIR spectroscopy and imaging of GRB 090205 with the ESO-VLT starting from hours after the event up to several days later to detect the host galaxy. We compared the results obtained from our optical/NIR observations with the available *Swift* high-energy data of this burst.
Results. Our observational campaign led to the detection of the optical afterglow and host galaxy of GRB 090205 and to the first measure of its redshift, $z = 4.65$. Similar to other, recent high-z GRBs, GRB 090205 has a short duration in the rest-frame with $T_{90,rf} = 1.6$ s, which suggests the possibility that it might belong to the short GRBs class. The X-ray afterglow of GRB 090205 shows a complex and interesting behaviour with a possible rebrightening at 500-1000s from the trigger time and late flaring activity. Photometric observations of the GRB 090205 host galaxy argue in favor of a starburst galaxy with a stellar population younger than ~ 150 Myr. Moreover, the metallicity of $Z > 0.27\,Z_{\odot}$ derived from the GRB afterglow spectrum is among the highest derived from GRB afterglow measurement at high-z, suggesting that the burst occured in a rather enriched enviroment. Finally, a detailed analysis of the afterglow spectrum shows the existence of a line corresponding to Lyman-α emission at the redshift of the burst. GRB 090205 is thus hosted in a typical Lyman-α emitter (LAE) at $z = 4.65$. This makes the GRB 090205 host the farthest GRB host galaxy, spectroscopically confirmed, detected to date.

Key words. gamma ray: bursts - gamma ray: individual GRB090205

1. Introduction

Gamma-Ray Bursts (GRBs) are powerful flashes of high-energy photons occuring at an average rate of a few per day throughout the Universe. Thanks to their optical brightness that typically overshines the luminosity of their host galaxy, they are detectable up to extremely high redshift, as clearly shown by the recent detection of GRB 090423 at $z \sim 8.2$ (Salvaterra et al. 2009; Tanvir et al. 2009). This has strengthened the idea that GRBs can be used as a tool to study the Universe up to (and beyond) the reionization epoch. Indeed, GRBs can be used to identify high-z galaxies and study their metal and dust content through the identification of metal absorption lines in their optical afterglow.

Two classes of GRBs, short and long, have been identified on the bases of their observed duration (shorter or longer than ~ 2 s) and spectral hardness (Kouveliotou et al. 1993). In the last years, observations by the *Swift* satellite has questioned this simple scheme calling for a classification invoking multiple observational criteria (see Zhang et al. 2009). To this end, prompt emission properties like the isotropic gamma-ray energy release ($E_{\gamma,iso}$) and the peak energy (E_p) seem to provide a promising tool for GRB's classification, as shown by the $E_{p,i} - E_{\gamma,iso}$ correlation (Amati et al. 2008) and its derivations (see, e.g., Lv et al. 2010 and references therein). While it is widely be-

Send offprint requests to: P. D'Avanzo, paolo.davanzo@brera.inaf.it

* The results reported in this paper are based on observations carried out at ESO telescopes under programmes Id 082.A-031 and 283.D-5033.

lieved that the majority of long GRBs originate from the collapse of massive stars, the nature of the progenitors of short ones is still unclear, though likely linked to the merger of two compact objects. Long GRBs are typically found to be hosted in low-mass, blue galaxies with high specific star formation rates (SSFR), whereas short GRBs are generally hosted in more heterogeneous types of galaxies, at least some with lower SSFR (see e.g. Fruchter et al. 2006; Berger 2009; Savaglio et al.2009; Fong et al. 2010).

In this paper we report the detection of GRB 090205 at $z = 4.65$ and the study of the properties of its host galaxy, a young starburst. The paper is organized as follows. In Section 2, we report the detection of GRB 090205 by *Swift* (Section 2.1) and the discovery and study of its optical afterglow and of its host galaxy (Section 2.2). The discussion about the nature of the burst is given in Section 3.1, whereas the interpretation of its afterglow is reported in Section 3.2. In Section 3.3, we discuss the nature of the host galaxy of GRB 090502 and finally, we summarize briefly our main conclusions in Section 4.

The standard cosmological parameters ($h = 0.71$, $\Omega_m = 0.27$, $\Omega_\Lambda = 0.73$) have been assumed and magnitudes are given in the AB system. All errors are at the 90% confidence level, unless stated otherwise.

2. Observations

2.1. Swift observation

GRB 090205 triggered *Swift*-BAT (Perri et al. 2009) on Feb. 2009, 5th at 23:03:14 UT (hereafter, T_0). The mask-weighted light curve shows a single peak starting at $T_0 - 5$ s, peaking at $T_0 + 3$ s, and returning to background at $T_0 + 100$ s (Fig. 1). The duration of the prompt emission is $T_{90} = 8.8 \pm 1.8$ s in the 15-150 keV band. The time-averaged spectrum from $T_0 - 2.9$ s to $T_0 + 6.6$ s in the 15-150 keV band can be fit by a simple power-law model with photon index $\Gamma = 2.15 \pm 0.23$. Alternatively, an equally good fit can be obtained by a cut-off power-law model with photon index $a = 0.8 \pm 1.3$ and observed peak energy $E_p = 34 \pm 15$ keV. A peak energy of $\sim$ 30 keV is also found from the relation between E_p and Γ obtained by Sakamoto et al. (2009). The fluence in the 15–150 keV band is $F_\gamma = (1.9 \pm 0.3) \times 10^{-7}$ erg cm^{-2} and the 1-s peak photon flux measured from $T_0 + 4.09$ s in the 15-150 keV band is $P = 0.5 \pm 0.1$ ph cm^{-2} s^{-1} (Cummings et al. 2009). Following the method described in Ukwatta et al. (2010), we performed the spectral lag analysis of the BAT data from $T_0 - 20$ s to $T_0 + 20$ s in four energy bands (12–25 keV, 25–50 keV, 50–100 keV, 100–350 keV) with a time bin of 1024 ms. All lags are consistent with zero, but with relatively large uncertainties, given the faintness of the prompt emission. *Swift*-XRT began to observe the field of GRB 090205 at $\sim$ 89 s after the trigger, identifying a fading uncatalogued X-ray source located at the UVOT-enhanced position RA (J2000): 14h 43m 38.69s and Dec (J2000): -27d 51′ 09.6″ with an uncertainty of 1.8″ (radius, 90% confidence, Evans et al. 2009). *Swift*-UVOT began settled observations of the field of GRB 090205 92 s after the BAT trigger, but no source was identified at the enhanced Swift XRT position. The burst was declared a "burst of interest" by Gehrels & Perri (2009).

2.1.1. XRT temporal and spectral analysis

The XRT data were processed with the XRTDAS software package (v.2.5.0) developed at the ASI Science Data Center (ASDC) and distributed by HEASARC within the HEASOFT package

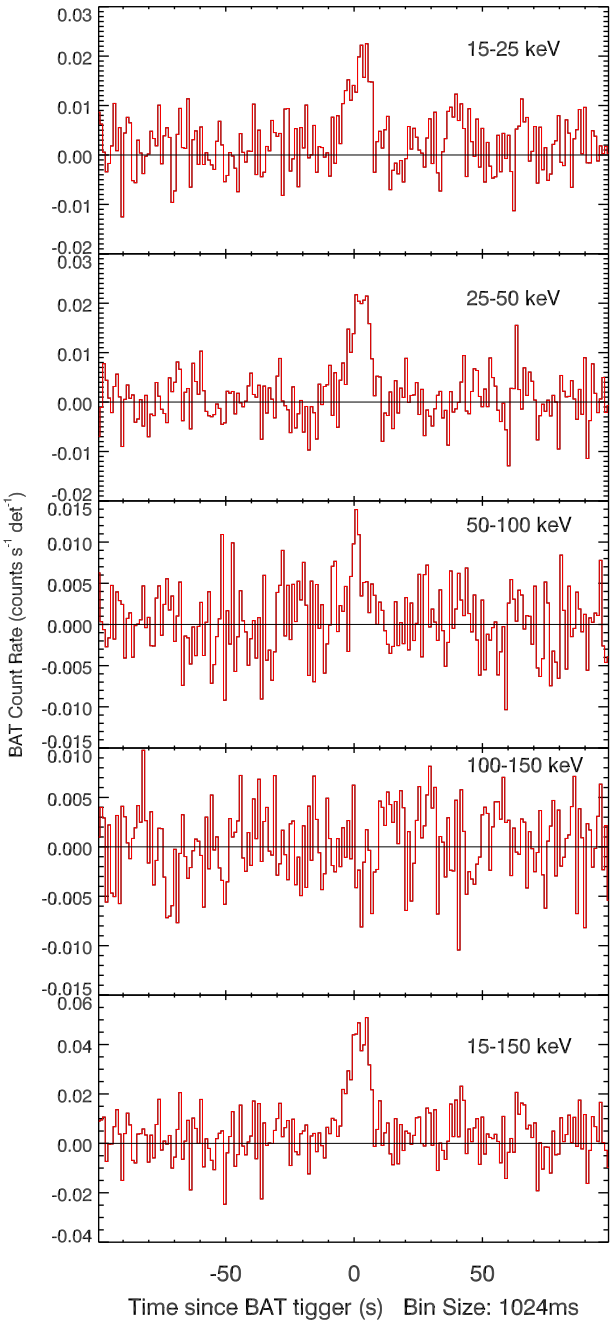

Fig. 1. Four channels and combined BAT mask-weighted light curve of GRB 090205. Bin size is 1024 ms.

(v. 6.7). Event files were calibrated and cleaned with standard filtering criteria with the *xrtpipeline* task using the latest calibration files available in the Swift CALDB. The X-ray light curve (Fig. 2) shows a complex behavior. At $\sim T_0 + 500$s, we note a possible re-brightening, while flaring activity is present at $\sim T_0 + 6$ ks and $\sim T_0 + 20$ ks, respectively. A fit with a double broken power-law ($F(t) \propto t^{-\alpha}$) gives indices $\alpha_1 = 1.36^{+0.37}_{-0.34}$ for $t < T_0 + t_{b,1}$, $\alpha_2 = -0.67^{+1.06}_{-0.66}$ for $T_0 + t_{b,1} < t < T_0 + t_{b,2}$, and $\alpha_3 = 1.15^{+0.09}_{-0.07}$ for $t > T_0 + t_{b,2}$ (excluding the flaring activity), where $t_{b,1} = 470^{+62}_{-82}$s and $t_{b,2} = 1039^{+245}_{-206}$s. We performed a time resolved spectral analysis of the X-ray afterglow during the first Swift orbit (spanning from $T_0 + 100$s to $T_0 + 2$

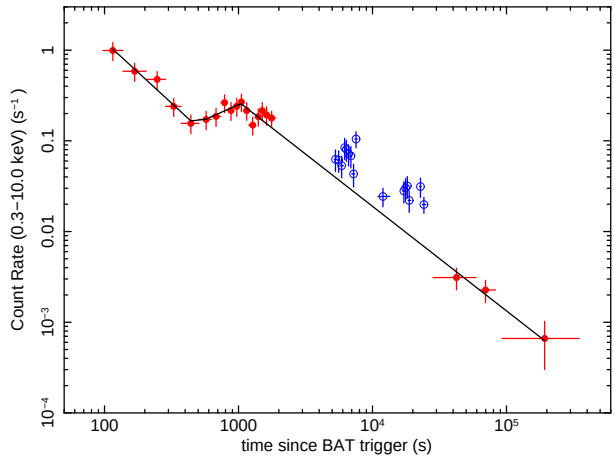

Fig. 2. X-ray light curve in count rate. The solid line shows the best power-law fit obtained excluding the flaring activity (marked by open circles) present at $\sim T_0 + 6$ ks and $\sim T_0 + 20$ ks, respectively. The conversion factor is 1 cts s^{-1} = 3.6×10^{-11} erg cm^{-2} s^{-1}. Errors are at 68% c.l.

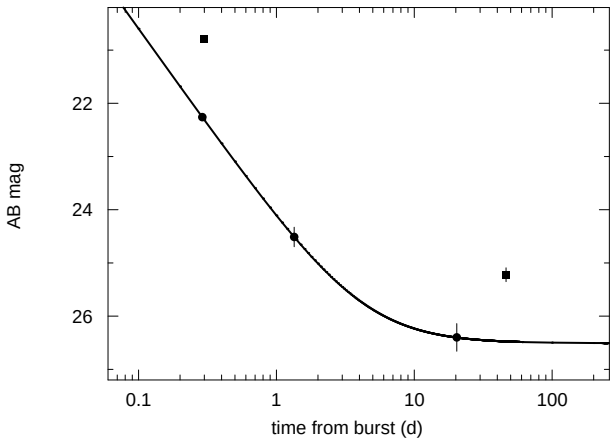

Fig. 3. Optical $R-$ (*dots*) and $I-$band (*squares*) afterglow light curve. The solid line shows the best power-law fit. Magnitude are in AB system and are not corrected for Galactic extinction. Errors are at 68% c.l.

ks) in three different time intervals: (i) $t < 470$s (initial decay), (ii) 470s< 1039s (rise phase of the re-brightening episode), and (iii) 1039s< $t < 2000$s (decay phase of the re-brightening episode). For all the three intervals the X-ray spectrum is well fitted by an absorbed power-law with photon index $\Gamma_X \sim 2.0$ ($\Gamma_{X,1} = 1.84 \pm 0.23, \Gamma_{X,2} = 2.00 \pm 0.24, \Gamma_{X,3} = 2.14 \pm 0.20$) and Galactic $N_H \sim 8 \times 10^{20}$ cm^{-2}, i.e. no spectral evolution is observed during the first orbit, although the data are compatible with a gradual softening of the spectrum. No evidence of intrinsic absorption at the redshift of the burst is found. The 2(3)-σ upper limit is $N_{H,z} < 2.3(3.5) \times 10^{22}$ cm^{-2}. These limits are obtained using the entire XRT dataset (i.e. using T_0+100 s – T_0+83 ks data). The time resolved spectral analysis of the X-ray flaring activity has been also obtained. The first time interval showing variability (from $T_0 + 5179$s to $T_0 + 7696$s) is well fitted by an absorbed power-law with photon index $\Gamma_X = 2.38 \pm 0.21$ and Galactic $N_H \sim 8 \times 10^{20}$ cm^{-2}, while for the second time interval (from $T_0 + 16782$s to $T_0 + 25067$s), there is some evidence of an harder spectrum with $\Gamma_X = 1.56 \pm 0.35$. We note, however, that during this flaring activity the photon index values are consistent (at the 90% CL) with the values measured at earlier times.

2.2. Optical/NIR observations

A complete log of all our optical/NIR ground based observations is reported in Tab. 1.

2.2.1. Optical/NIR imaging

We observed the field of GRB 090205 with the ESO-VLT in imaging mode starting about 7.1 hours after the burst. Observations were carried out in R and $I-$band with the FORS1 camera. Within the enhanced X-ray position, we identified a source at the following coordinates: RA(J2000)=14h 43m 38.70s and Dec(J2000)=-27d 51′ 10.0″ with an uncertainty of 0.3″ (D'Avanzo et al. 2009a). The source is detected in both bands with $R_{AB} = 22.26 \pm 0.04$ and $I_{AB} = 20.80 \pm 0.02$, the red color suggesting a high redshift object. All values given here are not corrected for Galactic extinction of $E(B-V) = 0.117$ (Schlegel et al. 1998). This result has been confirmed by almost contemporary GROND observations (Kruehler & Greiner 2009): the object is very well detected in the i'-band, marginally in the r'-band and not in the g'-band. Interpreting the non detection in the g'-band and the large $r' - i'$ color as due to Lyman-α absorption in the GRB host, a photometric redshift of 4.7 ± 0.3 has been derived.

We continued to follow the fading of the GRB afterglow with the FORS1 camera on VLT. A second epoch image was obtained ∼ 1.34 days after the trigger in the $R-$band (D'Avanzo et al. 2009b). The source is detected with $R_{AB} = 24.51 \pm 0.18$. The fading behaviour confirms it as the optical afterglow of GRB 090205. Late time, multiband observations were also carried out to search for the GRB host galaxy, showing a flattening in the R and, possibly, in the $I-$band light curves (see Sect 2.2.3). Assuming a power-law decay $F(t) = F_0 + kt^{-\alpha}$, the decay index is $\alpha_{opt} = 1.35^{+0.26}_{-0.19}$, steeper (but consistent within the errors) than the decay index derived from the X-ray light curve at the same epochs. A plot of our $R-$ and $I-$band observations is shown in Fig. 3.

2.2.2. Spectroscopic Observations

We observed the source with the ESO VLT about 9.0 hours after the burst with the FORS1 camera in spectroscopic mode. We took a 20 min spectrum with the 300V grism (11 Å FWHM) using a slit with 1″ width. We covered wavelength range 4000-10000 Å with a resolution of R=440 (Thöne et al. 2009; Fugazza et al. 2009). The spectrum was reduced with standard tasks in IRAF, combined and flux calibrated using observations of the standard star EG274 taken on Feb. 7, 2009.

The most prominent feature in the spectrum is the Damped Lyman Alpha system (DLA) at 6873 Å in the observer frame. Furthermore, we detect Ly−β and Ly−γ in absorption as well as the Lyman break. Redwards of the DLA, we detect a range of absorption lines from the host galaxy, SII, SiII, CII, SiIV and CIV (see Table 2). We also detect the fine structure transition of SiII* λ1264 Å, but no other fine structure lines could be identified. From those lines, we determine the redshift of the GRB to z= 4.6503 ± 0.0025. A plot of the combined spectrum with the lines identified is shown in Fig. 4. A detailed analysis of the spectrum shows the presence of an emission line at ∼ 6873 Å (Fig. 5). At the redshift of the GRB, it corresponds to Ly−α

Table 1. VLT observation log for GRB 090205.

Mean time (UT)	Exposure time (s)	Time since GRB (days)	Seeing ($''$)	Instrument	Magnitude	Filter
2009 Feb 06.25042	2×180	00.28984	0.7	VLT/FORS1	22.26 ± 0.04	R
2009 Feb 06.25751	2×180	00.29693	0.7	VLT/FORS1	20.80 ± 0.02	I
2009 Feb 07.30501	4×180	01.34443	1.0	VLT/FORS1	24.51 ± 0.18	R
2009 Feb 26.29729	7×180	20.33671	0.9	VLT/FORS1	26.40 ± 0.26	R
2009 Mar 11.36257	40×120	33.40199	0.7	VLT/FORS1	–	I
2009 Mar 24.22352	20×180	46.26294	0.7	VLT/FORS1	25.22 ± 0.13	I
2009 Mar 28.42134	$2 \times 30 \times 18$	50.46076	0.8	VLT/ISAAC	> 23.3	J
2009 Aug 10.02094	$4 \times 15 \times 64$	185.06036	0.9	VLT/HAWKI	> 24.4	J
2009 Aug 10.52803	$4 \times 15 \times 65$	185.56745	0.8	VLT/HAWKI	> 23.9	Ks
2009 Aug 11.02510	$4 \times 15 \times 65$	186.06452	0.6	VLT/HAWKI	> 24.2	H
2009 Feb 06.36422	1×1200	00.40364	0.7	VLT/FORS1	–	$300V + GG375$

Notes. Magnitudes are in the AB system and are not corrected for Galactic absorption. Errors and upper limits are given at 1σ and 3σ confidence level respectively.

emission at 1215 Å. We will discuss it more in detail in the next section.

We fitted the red wing of the DLA using the MIDAS fitlyman package. The resulting column density was determined to be log N_H/cm^{-2} =20.73±0.05. The HI column density lies below the average neutral hydrogen column density for GRB-DLAs of log N_H/cm^{-2} =21.6 (Jakobsson et al. 2006; Fynbo et al. 2009). This is in agreement with the simulations of Nagamine et al. (2008) which show that the mean DLA column density decreases with increasing redshift. On the other hand, the relatively low number of GRBs at redshift $\geq 3-4$ with measured HI column density and the probable observational bias against the most dusty environments (Jakobsson et al. 2006; Fynbo et al. 2009) do not enable yet to firmly check the existence of this anti-correlation.

The majority of the absorption lines detected are saturated and therefore do not allow a reliable determination of the column density. Mildly saturated lines, which we define here as lines with an EW of < 0.5 Å, do not lie on the linear part of the curve of growth and the derived column densities can only be considered as lower limits. For SII, SiII* and OI (EWs from 0.30 to 0.49, Tab. 2) we obtain, assuming a linear relation between the EW and the column density, log N/cm^{-2} =15.3, log N/cm^{-2} =13.4 and log N/cm^{-2} =14.8, respectively. We take the column density limit derived from SII to determine the metallicity of the host as SII is not affected by depletion onto dust. Using the solar abundances reported in Asplund et al. (2009), we find the metallicity in the host along the line of sight to be $[M/H] > -0.57$ or $Z > 0.27\ Z_\odot$.

Table 2. Measured wavelengths, derived redshift and equivalent widths (EWs) of detected absorption lines

λ_{obs} [Å]	λ_{rest} [Å]	id	z	EW_{rest} [Å]	log N [cm^{-2}]
5495	972.54	Lyγ	—	—	—
5791	1025.72	Lyβ	—	—	—
6870	1215.67	Ly−α	—	98.5	20.73±0.05
7091.20	1253.81	SII	4.6557	0.30	>15.3
7120.35	1259.52	SII	—	1.38±0.04	—
—	1260.42	SiII	—	*blended*	—
—	1260.53	FeII	—	*blended*	—
7149.40	1264.74	SiII*	4.6529	0.42±0.03	>13.4
7357.65	1302.17	OI	4.6503	0.49±0.02	>14.8
7372.76	1304.37	SiII	4.6523	0.95±0.04	—
7543.54	1334.53	CII	—	1.96±0.50	—
—	1335.71	CII	—	*blended*	—
7873.45	1393.76	SiIV	4.6490	2.07±0.16	—
7919.98	1402.77	SiIV	4.6460	3.91±0.51	—
8627.73	1526.71	SiII	4.6512	1.36±0.04	—
8754.28	1550.78	CIV	4.6450	2.89±0.04	—

Notes. The EW for the blended systems include the contributions from all transitions in the blended line. For blended systems, the redshift is not mentioned due to the large uncertainty. We only give lower limits on the column density for mildly saturated lines which we define here as EW < 0.5 Å in the restframe.

2.2.3. Host galaxy observations

We continued to monitor the field of GRB 090205 at late times to further study the GRB host. We obtained an image in the $R-$band with the FORS1 camera $\sim$ 20.3 days after the trigger. A faint object at a magnitude of $R_{AB} \sim 26.4 \pm 0.3$ has been identified very close to the position of the GRB afterglow. This detection represents a flattening in the $R-$band light curve, that we interpret as due to the host galaxy (Fig. 3). Further $I-$band monitoring, carried out $\sim$ 46.3 days after burst[1] reveals an object with $I_{AB} = 25.2 \pm 0.1$. Comparing this detection with the previous one obtained in the $R-$band, the resulting unabsorbed $R-I$ color is consistent with that of the afterglow. This suggests a flattening of the light curve in the $I-$band too, in agreement with the hypothesis that we detected the host galaxy of GRB 090205. We also carried out deep, late-time ($t - T_0 \sim 180$ d) NIR observations of the field of GRB 090205 with VLT/HAWK-I in $JHK-$bands. The host is not detected in any of the observed bands up to a limiting AB magnitude of $J > 24.4$, $H > 24.2$ and $Ks > 23.9$ (3σ c.l.). The results are reported in Tab. 1 and in Figs. 6,7.

As already mentioned, the afterglow spectrum shows an emission line at $\sim$ 6873 Å superposed on the Ly-α absorption, corresponding to Ly-α emission at the same redshift of the GRB. In order to check the reliability of the line detection, and to exclude the possibility that it is due to some atmospheric emission or absorption contaminating feature, we performed a detailed analysis of the 2-D spectrum (see Fig. 5). At the wavelength corresponding to the Ly−α line emission we measure 2101 ± 51 counts (sky+object). The counts corresponding only

[1] As reported in Tab. 1, another epoch of $I-$band imaging was taken at $t - T_0 \sim 33$ d but, erroneously, no dithering was performed among different frames. The resulting image was thus highly affected by fringing (see http://www.eso.org/sci/facilities/paranal/instruments/fors/) and it was not possible to obtain reliable measures of photometry.

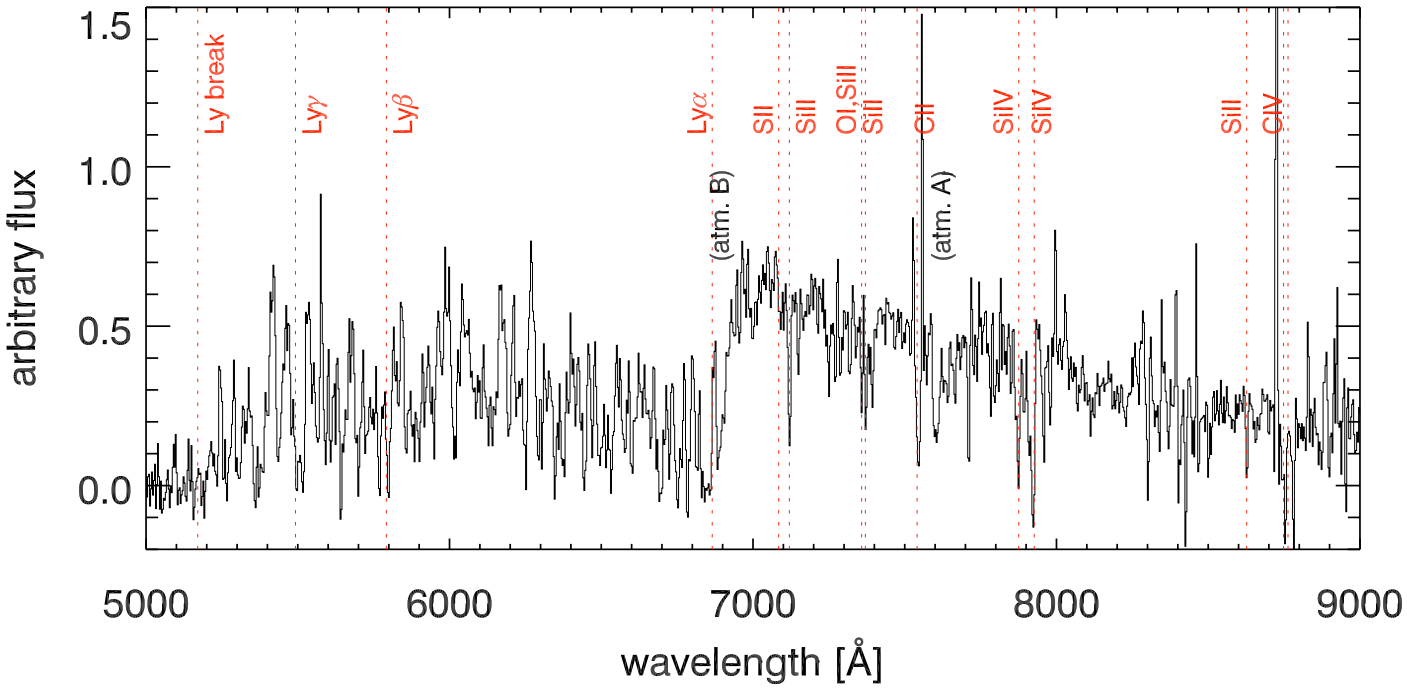

Fig. 4. VLT/FORS1 spectrum of the GRB 090205 afterglow at $z = 4.6503 \pm 0.0025$.

to sky are 1836 ± 21, so that the object counts are 265 ± 55 (68% c.l.). The corresponding signal-to-noise ratio is 5.2. Another striking evidence we obtain from the 2-D spectrum is the measure of a spatial displacement of 1.3 ± 0.9 pixels (equivalent to $0.3'' \pm 0.2''$) from the centroid of the afterglow continuum trace and the "spot" corresponding to the Ly−α emission (see Fig. 5). Doing precise astrometry on our afterglow and host galaxy images obtained with FORS1, we measure the same offset between the afterglow and the host galaxy positions ($0.4'' \pm 0.3''$, corresponding to a physical offset of about 3 kpc), thus making stronger the hypothesis that this emission line is really due to Ly−α from the host galaxy. Using the flux-calibrated afterglow spectrum we derive a flux of 1.82×10^{-17} erg s^{-1} cm^{-2}. This flux transforms into a Ly−α luminosity of 4.27×10^{42} erg s^{-1}. We note that this value is in the range of luminosities observed for the other GRB-LAE hosts[2], i.e. $1 - 5 \times 10^{42}$ erg s^{-1} (Jakobsson et al. 2005).

3. Discussion

3.1. Burst classification

One interesting aspect of this burst is that, similarly to other, high-z GRBs (e.g. GRB 080913 at $z = 6.7$, Greiner et al. 2009; GRB 090423 at $z = 8.2$, Salvaterra et al. 2009, Tanvir et al. 2009), it shows a short duration in the emitter rest frame, $T_{90,rf} \sim 1.6$ s. A short rest frame duration was recently proposed as a possible indicator (among others) of GRBs originated from a compact-star-merger progenitor (or Type I GRBs; Zhang et al. 2009). While the spectral lag analysis is inconclusive regarding the nature of this burst, owing to the faintness of the prompt emission (Sec. 2.1), the BAT spectrum appears to be softer with respect to typical short GRBs. At $z = 4.65$, the isotropic gamma-ray energy release in the redshifted 15-150 keV band is $E_{\gamma,iso} = 7.86 \pm 1.21 \times 10^{51}$ erg and the intrinsic peak energy is $E_{p,i} = 192 \pm 85$ keV. These values make GRB 090205 consistent with the observed $E_{p,i} - E_{\gamma,iso}$ correlation (Amati et al. 2008), that is known to be followed only by long GRBs (see also Piranomonte et al. 2008) and proposed as an indicator of GRBs with a massive stellar collapse origin (Type II GRBs; Zhang et al. 2009). Indeed, the $E_{p,i} - E_{\gamma,iso}$ correlation has been used recently to support the long classification of a few rest-frame short duration bursts such as GRB 090423 (Salvaterra et al. 2009) and GRB 090426 (Antonelli et al. 2009). A Type II classification for GRB 090205 is also supported by applying the classification method reported in Lv et al. (2010), being $\epsilon = E_{\gamma,iso,52}/{E_{p,z,2}}^{5/3} \sim 0.26$, where $E_{\gamma,iso,52} = E_{\gamma,iso}/10^{52}$ erg and $E_{p,z,2} = E_p(1+z)/10^2$ keV. This value puts GRB 090205 in the high-ϵ regime, which is related to long (Type II) GRBs.

In conclusion, even if a massive stellar collapse origin for GRB 090205 may appear puzzling (although not unheard of)[3] in light of its rest frame short duration, the prompt emission properties of this GRB favors for a Type II classification. Furthermore, we note that, while the existence at high-z of a population of bursts originating from the merging of double compact objects is expected on theoretical ground (Belczynski et al. 2010), their detection would imply a very flat luminosity function for the short burst population, in contrast with a recent analysis of BATSE and *Swift* data (Salvaterra et al. 2008).

3.2. Afterglow theoretical interpretation

As shown in Sect. 2.1, the X-ray afterglow evolution can be divided into three stages. The closure relation for the first stage is $\alpha_1 - 1.5\beta_1 = 0.10^{+0.51}_{-0.48}$, which can not constrain any model due to the large scatter of the error bars. The closure relation for the

[2] GRB 971214 ($z = 3.42$), GRB 000926 ($z = 2.04$), GRB 011211 ($z = 2.14$), GRB 021004 ($z = 2.33$), GRB 030323 ($z = 2.66$), and GRB 030429 ($z = 2.66$).

[3] Despite their short rest-frame duration, the high−z GRB 080913 and GRB 090423 were classified as Type II bursts (Zhang et al. 2009).

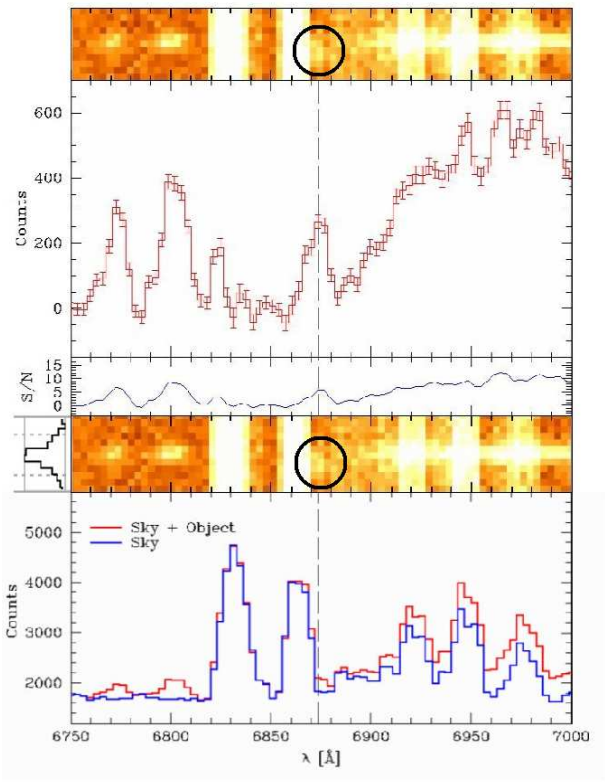

Fig. 5. Detailed analysis of the Ly−α emission line detection. The top panel shows the blow up of the region centered on the Ly−α emission at 6873.45Å (dashed line), corresponding to 1215.67Å in the emitter rest frame. The central panel shows the corresponding signal-to-noise ratio. The bottom panel reports the counts from the sky (blue line) and for the sky+object (red line). The position of the Ly−α emission in the 2-D spectrum (shown in both panels), is marked by a circle and has an offset with respect to the afterglow continuum (corresponding to 0.3″; see Sec. 2.2.3 for details).

third stage is $\alpha_3 - 1.5\beta_3 = -0.56 \pm 0.31$, quite consistent with the theoretical expectation of $\alpha - 1.5\beta = -0.5$, where $\alpha = (3p-2)/4$ and $\beta = p/2$. Therefore, for $t > 10^3$ s, the inferred power law index of electron energy distribution shaped by shock acceleration is $p = 2.20^{+0.12}_{-0.09}$. Therefore, the simplest forward shock model for the first and third stages corresponds to the X-ray band being above the cooling and typical frequencies of synchrotron radiation, i.e., $\nu_x > max(\nu_m, \nu_c)$.

The second stage shows a rise of the X-ray flux with time. Interpreting it as due to the emergence of the Synchrotron-Self-Compton component in the X-ray band, there should be significant spectral hardening around the transition time $t \sim 500$ s, which is contrary to what we observed. Alternatively, the rise may be due to the continuous energy injection ($L_{\rm inj} \propto t^{-q}$) from late time central engine activities (e.g., Dai & Lu 1998) or refreshed shock (Rees & Meszaros 1992) by a late time ejecta with varying Lorentz factors within the ejecta ($M(>\Gamma) \propto \Gamma^{-s}$). Since the X-ray spectral index in the rising phase is steep, the characteristic frequencies ν_c and ν_m should be below the X-ray band. According to Table 2 of Zhang et al. (2006), we use the relation of $\alpha_2 = (q-2)/2 + (q+2)\beta_2/2$ and obtain $q = 2(1+\alpha_2-\beta_2)/(1+\beta_2) = -0.67^{+1.07}_{-0.68}$, where $\alpha_2 = -0.67^{+1.06}_{-0.66}$ and $\beta_2 = 1.00 \pm 0.24$. For the matter-dominated injection model, $s = (10-7q)/(2+q) = 11.05^{+9.23}_{-14.52}$ for the ISM case and $s = 4/q - 3 = -8.97^{+6.06}_{-9.53}$ for the wind case. Since $s < 0$ is unphysical, the wind model is therefore not favored if the rebrightening is due to a matter-dominated refreshed shock. The afterglow kinetic energy after the rising phase is increased by a factor of $\left(\frac{1000\ \rm s}{500\ \rm s}\right)^{1-q} \sim 3.2^{+3.5}_{-1.2}$.

The X-ray afterglow clearly shows the presence of late-time temporal variability (4 ks < t < 20 ks). The variable afterglow is characterised by a flux contrast $\Delta F/F \sim 3$, where ΔF is the flux enhancement due to the possible flares and F is the flux level of the underlying continuum. This together with the upper limit on the variability ratio $\Delta t/t < 0.3$, places the GRB 090205 possible X-ray flares at the boundary between density fluctuations produced by many regions viewed off-axis and refreshed shocks (see Ioka et al. 2005; Chincarini et al. 2007, their Fig. 15). However, the low statistics prevents us from drawing quantitative conclusions on both the temporal (see Chincarini et al., 2010 for an updated analysis on 113 GRB X-ray flares) and spectral behaviour of this possible flaring activity (Falcone et al. 2007).

The Galactic extinction corrected I-band flux density at $t \sim 25$ ks is $\sim 21.4\ \mu$Jy. At this time, the 0.3 - 10 keV count rate is $\sim 6.3 \times 10^{-3}$ counts s^{-1}, corresponding to a flux of 2.3×10^{-13} erg cm^{-2} s^{-1}. Assuming the late-time X-ray spectral index $\beta_3 = 1.07$, the X-ray flux density at $\nu_X = 10^{18}$ Hz is $\sim 6.2 \times 10^{-3}\ \mu$Jy. So the near infrared to X-ray overall spectral index at $t \sim 25$ ks is $\beta_{NIR-X} \sim 1.0$, suggesting that the optical/NIR and the X-ray emission are from the same origin.

In conclusion, the X-ray and optical afterglow can be explained within the standard forward shock model with $\nu_c, \nu_m < \nu_{\rm opt}$ and ν_X. The early rebrightening in the X-ray afterglow can be interpreted as due to the energy injection into the forward shock by the central engine. We note that more complex modelling of the rebrightening phase (i.e. two-component models) are not strictly required by the data.

3.3. GRB host

Our photometric campaign carried out with VLT/FORS, ISAAC and HAWK-I (see Sect. 2.2.3) allows us to detect the GRB host galaxy in the R and I band and to put strong upper limits on the continuum in the NIR bands (J, H, and K). The observed magnitude and limits are reported in Table 1 and shown in Figs. 6,7. The blue color, $(I-K)_{AB} < 1.1$, argues for a starburst galaxy, whereas ellipticals, Sab, Scd type of galaxy are discarded (see Fig. 6). We therefore model the photometric data with a family of synthetic starburst SEDs computed from the outputs of the Starburst99 code (Leitherer et al. 1999; Vazquez & Leitherer 2005). We adopt a Salpeter initial mass function in the mass range 0.1-100 $M_\odot$ and a metallicity of $Z = 0.4\ Z_\odot$ consistently with the metallicity obtained from the GRB afterglow spectrum. Different ages of the stellar population are considered and the synthetic SEDs are normalized to reproduce the observed magnitude in the I-band. The absorption due to the intergalactic medium shortwards the Ly−α has been modelled as in Salvaterra & Ferrara (2003, see Section 2.2). The theoretical SEDs are shown in Fig. 7 from top to bottom with stellar ages of 500, 100, 50, 10 Myr, respectively. We find that the upper limits in the NIR bands provide a strong limit to the age of the stellar population. In order not to exceed the J and K band upper limits, the stellar population should be younger than $\tau < 150$ Myr. In this case, the corresponding stellar mass is $M_\star < 5 \times 10^{10}\ M_\odot$, in agreement with average mass of long GRB host galaxies ($10^{8.5} - 10^{10.3}\ M_\odot$ Savaglio et al. 2009). We neglect here the possible presence of

dust inside the host galaxy. However, we note that dust extinction would result in a reddening of the host SED, strengthening our limits on the stellar age and mass.

As described in Sect. 2.2.3, we found evidence that the host galaxy of GRB 090205 is a Ly−α emitter. The Ly−α emission line lies at $z = 4.6537 \pm 0.0014$ that, compared to the redshift measured from the absorption lines (Sec. 2.2.2), gives $\Delta z = 0.0034 \pm 0.0029$ ($\Delta v = 180 \pm 153$ km s^{-1}). This is in line with the results obtained through spectroscopic studies performed on large samples of Lyman break galaxies (LBG) at $z \sim 3$ that show velocity offsets between the Ly−α emission and interstellar absorption line redshifts of the order of ~ 600 km s^{-1}, with large dispersion ($\sim 300-500$ km s^{-1}; see e.g. Adelberger et al. 2003; Shapley et al. 2003; Bielby et al. 2010). Such kinematics is usually interpreted as due to large-scale outflows caused by supernova–driven wind, resulting from intense star formation, that blueshift absorption lines from the interstellar gas. At the redshift of the burst, the Ly−α luminosity is 4.3×10^{42} erg s^{-1}. This value lies in the range of luminosities of other LAEs identified by dedicated surveys at $z \sim 4.5$ (Finkelstein et al. 2007; Shioya et al. 2009; Wang et al. 2009). In particular, Shioya et al. (2009) in a recent survey of $z \sim 4.8$ LAE in the COSMOS 2 square degree field compute the Ly−α luminosity function of these objects, measuring $L_\star = 8^{+17}_{-4} \times 10^{42}$ erg s^{-1}. Similarly, Wang et al. (2009) find $L_\star = 6.3 \pm 1.5 \times 10^{42}$ erg s^{-1} for a sample of 110 LAEs detected in the Large Area Lyman Alpha (LALA) survey. Our findings suggest thus that this burst exploded into a 0.6-0.7 $L_\star$ LAE at that redshift. Transforming the luminosity in a star-formation rate using the formula from Kennicutt (1998) for Hα and assuming a factor of 8 between Hα and Ly−α, we derive a SFR of 4.2 M$_\odot$ yr^{-1} which is among the typical values found for other Ly-α emitters hosting GRBs (see, e.g. Jakobsson et al. 2005) and typical galaxies hosting GRBs (Savaglio et al. 2009). However the above values should be interpreted as lower limits. During the acquisition of the spectrum, the slit was centered on the afterglow position, so that we lost part (about 50%) of the Ly−α flux coming from the host galaxy, due to the 0.4″ offset we discussed in Sec. 2.2.3.

Our analysis of the GRB afterglow spectrum provides also a lower limit on the galaxy metallicity, $Z \geq 0.27\ Z_\odot$. Given the limit on the stellar mass obtained above, this metallicity is consistent with the mass-metallicity measured for Lyman Break Galaxies at $z = 3 - 4$ (Mannucci et al. 2009). We caution however that the metallicity probed by absorption lines does not necessarily probe the metallicity of the entire GRB host, but more likely of the line of sight towards the inner, star-forming region of the GRB host. The metallicity of GRB 090205 is among the highest determined for high-z GRBs. Comparing the metallicity of GRB 090205 to those determined for other GRBs at various redshifts, we find little or no evolution with redshift, in contrast with what found for the QSO selected DLA population (Fynbo et al. 2006; Savaglio et al. 2009).

4. Conclusions

We report the detection and study of GRB 090205 at $z = 4.65$. Similar to other, recent high-z GRBs, GRB 090205 has a short duration in the rest-frame with $T_{90,rf} = 1.6$ s. However, the analysis of its prompt emission properties favor a massive stellar collapse origin. The X-ray afterglow of GRB 090205 shows a complex behaviour with a possible rebrightening at 500-1000s from the trigger and flaring activity at later times. The X-ray and optical afterglow can be explained within the standard forward shock model with $\nu_c, \nu_m < \nu_{\rm opt}$ and ν_X, where the early rebrightening

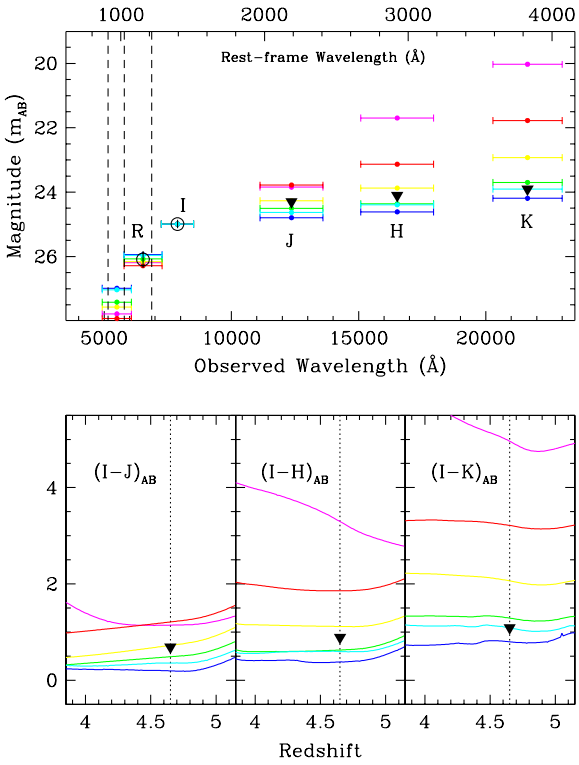

Fig. 6. Top panel: available data and expected magnitude of the GRB 090205 host for different galaxy types. The SEDs are normalized to reproduce the I band measure. Open circles (filled triangles) represent the data (upper limits), whereas the horizontal lines show the expected AB apparent magnitude of the object in the $VRIJHK$ bands for different host galaxy types: magenta is for Elliptical, red for Sab, yellow for Scd, green for Irregular, cyan and blue for starburst galaxies. Vertical lines mark the position of Lyman limit, Lyβ and Ly−α (from left to right), respectively. Bottom panels: expected $(I-J)$, $(I-H)$ and $(I-K)$ colors for the different galaxy types. Observational limit on the colors are plotted with triangles.

in the X-ray afterglow can be interpreted as due to the energy injection into the forward shock by the central engine.

Finally, we report the detection of the host galaxy of GRB 090205, which is found to be a typical LAE at $z = 4.65$, making it the farthest GRB host galaxy spectroscopically confirmed. The blue color indicates a starburst galaxy with a young ($\tau < 150$ Myr) stellar population, further supporting the long classification for this GRB. The obtained mass and SFR are in line with typical values of GRB host galaxies, while the metallicity derived from the GRB afterglow spectrum is among the highest derived from GRB afterglow measurement at high-z, suggesting that the burst occured in a rather enriched envirorment.

In conclusion, GRB 090205 clearly shows that GRBs can be used as signpost of young, starburst galaxies at high-z that are thought to be the dominant galaxy population at those epochs. Thanks to the brightness of their afterglow, metal lines can be easily identified providing, together with follow-up photometric observation of their host galaxies, a new way to measure the mass-metallicity relation and its evolution through cosmic times.

Acknowledgements. We thank the referee for his/her useful comments and suggestions. We acknowledge support by ASI grant SWIFT I/011/07/0. This research has made use of the XRT Data Analysis Software (XRTDAS) developed

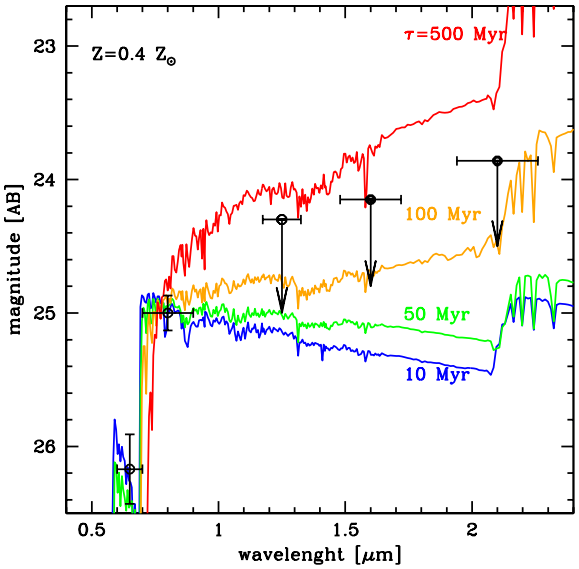

Fig. 7. Observations of the host galaxy of GRB 090205 shown with data points and upper limits are compared with synthetic SEDs for a starburst galaxy with different stellar ages τ. From top to bottom, lines corresponds to τ = 500, 100, 50, 10 Myr, respectively. We assume a Salpeter IMF between 0.1-100 $M_{\odot}$, Z = 0.4 $Z_{\odot}$ and no dust extinction in the host galaxy. The SED are normalized to reproduce the observation in the I band.

under the responsibility of the ASI Science Data Center (ASDC), Italy. We acknowledge the invaluable help from the ESO staff at Paranal in carrying out our target-of-opportunity observations.

References

Adelberger, K. L., Steidel, C. C., Shapley, A. E. & Pettini, M., 2003, ApJ, 584, 45
Amati, L., Guidorzi, C. Frontera, F. et al., 2008, MNRAS, 391, 577
Antonelli, L. A., D'Avanzo, P., Perna, R. et al., 2009, A&A, 507, L45
Asplund, M., Grevesse, N., Sauval, A. J., Scott, P., 2009, ARA&A, 47, 481
Belczynski, K., Holz, D. E., Fryer, C. L. et al., 2010, ApJ, 708, 117
Berger, E., 2009, ApJ, 690, 231
Bielby, R., Shanks, T., Weilbacher, P. M. et al., 2010, arXiv:1005.3028
Chincarini, G., Moretti, A., Romano, P. et al. 2007, ApJ 671, 1903
Chincarini, G., Mao, J., Margutti, R., et al., 2010, submitted to MNRAS, arXiv:1004.0901
Cummings, J. R., Barthelmy, S. D., Baumgartner, W. H. et al., 2009, GCN Circular, 8886
Dai, Z. G. & Lu, T. 1998, A&A, 333, L87
D'Avanzo, P., Thöne, C. C., Fugazza, D. et al. 2009a, GCN Circular, 8887
D'Avanzo, P., Fugazza, D., D'Elia, V. et al. 2009b, GCN Circular, 8895
Evans, P. A., Goad, M. R., Osborne, J.P., Beardmore A.P. 2009, GCN Circular, 8885
Falcone,A. D., Morris, D., Racusin, J. et al. 2007, ApJ, 671, 1921
Finkelstein, S. L., Rhoads, J. E., Malhotra, S., Pirzkal, N., Wang, J. X. 2007, ApJ, 660, 1023
Fong, W., Berger, E., Fox, D. B. 2010, ApJ, 708, 9
Fruchter, A. S., Levan, A. J., Strolger, L. et al. 2006, Nature, 441, 463
Fugazza, D., Thöne, C. C., D'Elia, V. et al. 2009, GCN Circular, 8892
Fynbo, J. P. U. Starling, R. L. C., Ledoux, C. et al., 2006, A&A, 451, L47
Fynbo, J. P. U., Jakobsson, P., Prochaska, J. X. et al., 2009, ApJS, 185, 526
Gehrels, N. & Perri, M., 2009, GCN Circular, 8890
Greiner, J., Kruehler, T., Fynbo, J. P. U. et al., 2009, ApJ, 693, 1610
Ioka, K., Kobayashi, S., Zhang, B. 2005, ApJ, 631, 429
Jakobsson, P., Björnsson, G., Fynbo, J. P. U. et al., 2005, MNRAS, 362, 245
Jakobsson P., Fynbo, J. P. U., Ledoux, C. et al. 2006, A&A, 460, L13
Kennicutt, R. C. Jr. 1998, ARA&A, 36, 189
Kouveliotou, C., Meegan, C. A., Fishman, G. J. et al., 1993, ApJ, 413, L101
Kruehler, T. & Greiner, J., 2009, GCN Circular, 8888
Leitherer, C., Schaerer, D., Goldader, J. D. et al., 1999, ApJS, 123, 3
Lv, H., Liang E., Zhang, B. -B., Zhang, B. 2010, submitted to ApJ, arXiv:1001.0598
Mannucci, F., Cresci, G., Maiolino, R. et al., 2009, MNRAS, 398, 1915
Nagamine, K., Zhang, B. & Hernquist, L. 2008, ApJL, 686, L57
Piranomonte, S., D'Avanzo, P., Covino, S. et al. 2008, A&A, 491, 183
Perri, M., et al. 2009, GCN Circular, 8884
Rees, M. J., Meszaros, P. 1992, MNRAS, 258, 41
Sakamoto, T., Sato, G., Barbier, L. et al., 2009, ApJ, 693, 922
Salvaterra, R., Cerruti A., Chincarini G. et al. 2008, MNRAS, 388, L6
Salvaterra, R. & Ferrara A., 2003, MNRAS. 339, 973
Salvaterra, R. Della Valle, M. Campana, S. et al., 2009, Nature, 461, 1258
Savaglio, S., Glazebrook, K., & LeBorgne, D. 2009, ApJ, 691, 182
Schlegel, D. J., Finkbeiner, D. P. & Davis, M., 1998, ApJS, 500, 525
Shapley A. E., Steidel, C. C., Pettini, M. & Adelberger, K. L., 2003, ApJ, 588, 65
Shioya, Y., Taniguchi, Y., Sasaki, S. S. et al. 2009, ApJ, 696, 546
Tanvir, N., Fox, D. B., Levan, A. J. et al., 2009, Nature, 461, 1254
Thöne, C. C., Fugazza, D. D'Avanzo, P. et al. 2009, GCN Circular, 8889
Ukwatta, T. N., Stamatikos, M., Dhuga, K. S. et al. 2010, ApJ, 711, 1073
Vazquez G. A. & Leitherer C., 2005, ApJ, 621, 695
Wang J.-X., Malhotra S., Rhoads J.E., Zhang H.-T., Finkelstein S. L., 2009, ApJ, 706, 762
Zhang, B., Fan, Y. Z., Dyks, J. et al., 2006, ApJ, 642, 354
Zhang, B., Zhang, B. -B., Virgili, F. J. et al., 2009, ApJ, 703, 1696